

Supporting Information

Active Vanadium(IV) Species Synthesized at Low-Temperature Facilitate Excellent Performance in Low-Temperature NO_x-Catalytic Removal

Liwei Sun,^a Peng Liu,^a Jianheng Xu,^b Kaijie Liu,^b Zeshu Zhang,^b Yibo Zhang^{*b} and Xiangguang Yang^{*b}

^a Changchun Institute of Applied Chemistry, Chinese Academy of Sciences, Changchun 130022, China

^b Ganjiang Innovation Academy, Chinese Academy of Sciences, Ganzhou 341000, China

General Characterizations

1. The **thermogravimetric analysis** (TG/DTA) was recorded on Seiko TG/DTA 6300.
2. The **powder X-ray diffraction** (XRD) patterns of the materials were recorded on a Rigaku D/Max 2550 X-ray diffractometer with Cu K α radiation ($\lambda = 1.5418 \text{ \AA}$).
3. The **transmission electron microscope** (TEM) images were obtained with a FEI Tecnai G² S-Twin microscope equipped with a field emission gun operating at 200 kV acceleration voltage. For each sample, the size of 200 particles was measured from multiple images randomly taken in different areas of the sample.
4. The **Raman** spectra were measured on Jobin-Yvon HORIBA Xplora confocal Raman system. The excitation wavelength is 638 nm and a 50-fold microscope objective with an aperture of 0.55 is used in all Raman measurements. The exciting power is controlled at about 1.5 mW.
5. The **temperature-programmed analysis** including reduction (TPR) and desorption (TPD) were carried out in Micromeritics 2920 analyzer.
6. The ⁵¹V **magic angle spinning solid-state nuclear magnetic resonance** (MAR NMR) was measured by Bruker AVANCE NEO NMR spectrometer.
7. The **X-ray photoelectron spectroscopy** (XPS) was performed using an ESCALAB 250 X-ray photoelectron spectrometer with a monochromatic X-ray source (Al K α $h\nu = 1486.6 \text{ eV}$). The energy scale of the spectrometer was calibrated using Au 4f_{7/2}, Cu 2p_{3/2}, and Ag 3d_{5/2} peak positions. The standard deviation for the binding energy (BE) values was 0.1 eV.

8. The Brunauer–Emmett–Teller (BET) surface area was measured using a Micromeritics ASAP 2020 instrument.

Additional Figures

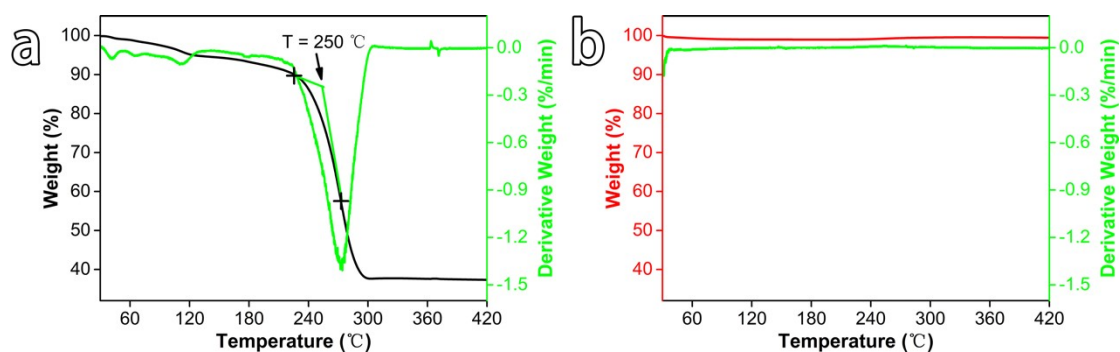


Figure S1. TG/DTA curves of (a) vanadium oxalate and (b) V_{260°C} catalysts.

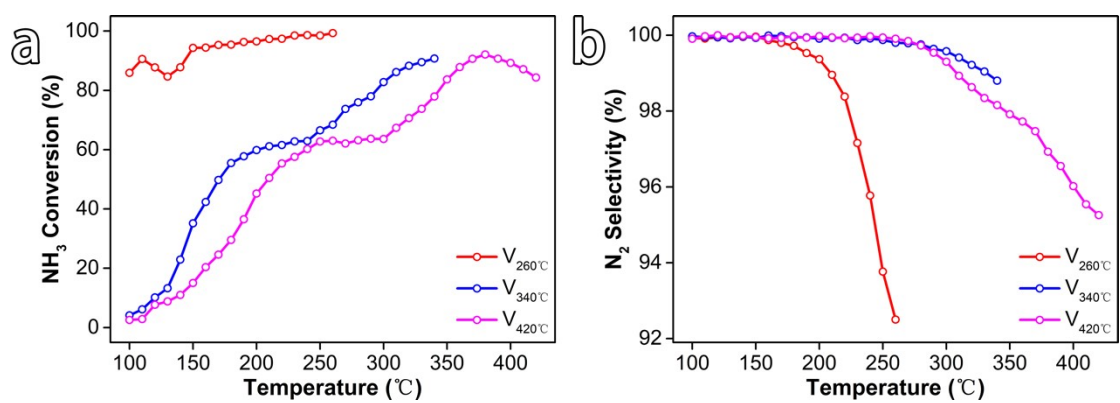


Figure S2. (a) NH₃ conversion and (b) N₂ selectivity of V_{260°C} (red), V_{340°C} (blue), and V_{420°C} (pink) catalysts.



Figure S3. Segmented reactor photo.

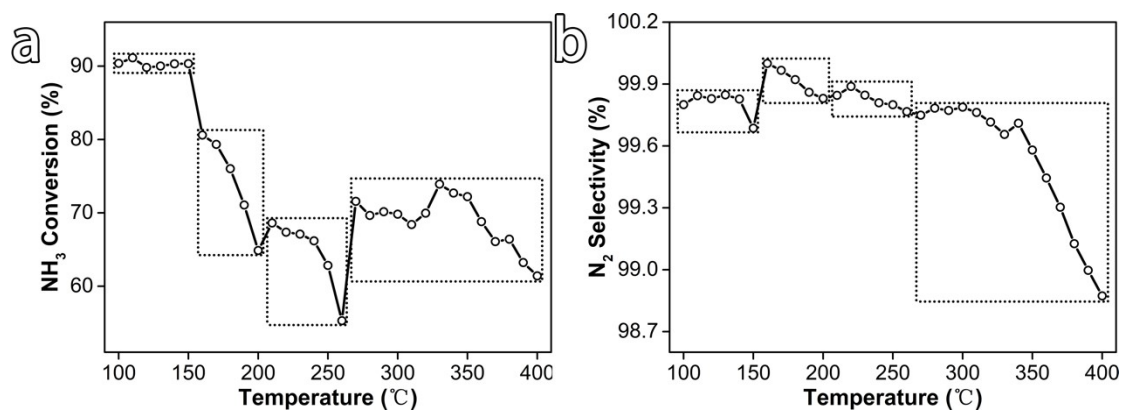


Figure S4. (a) NH_3 conversion and (b) N_2 selectivity of the segmented catalyst in an appropriate ratio ($V_{420^\circ\text{C}}:V_{420^\circ\text{C}}:V_{340^\circ\text{C}}:V_{260^\circ\text{C}} = 1:1:1:7$ (wt %))

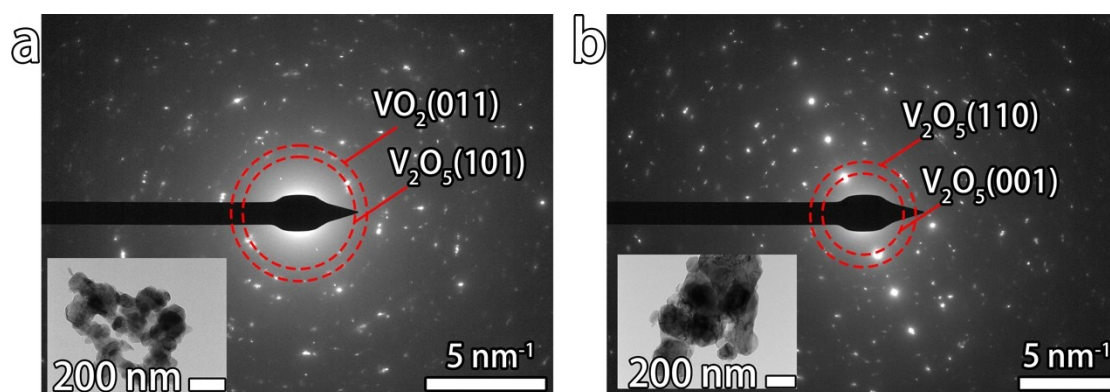


Figure S5. TEM of (a) $V_{340^\circ\text{C}}$ and (b) $V_{420^\circ\text{C}}$ catalysts.

Table S1. N₂ physical adsorption results for bulk vanadium oxide catalysts

Catalyst	V _{260°C}	V _{340°C}	V _{420°C}
BET (m ² ·g ⁻¹)	28.3	10.5	6.2

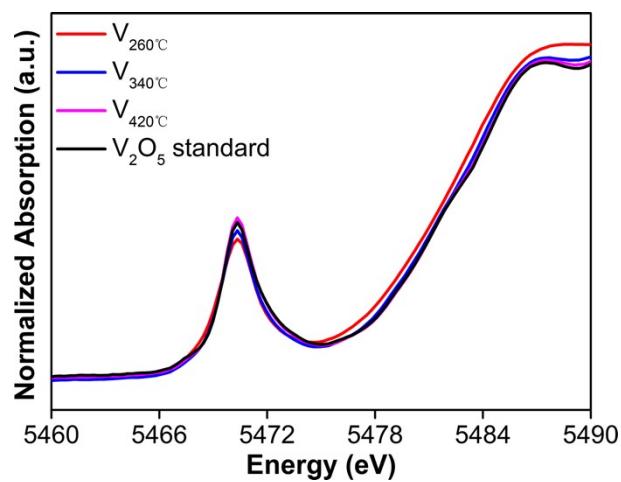


Figure S6. EXAFS spectra of the V_{260°C}, V_{340°C}, and V_{420°C} catalysts.

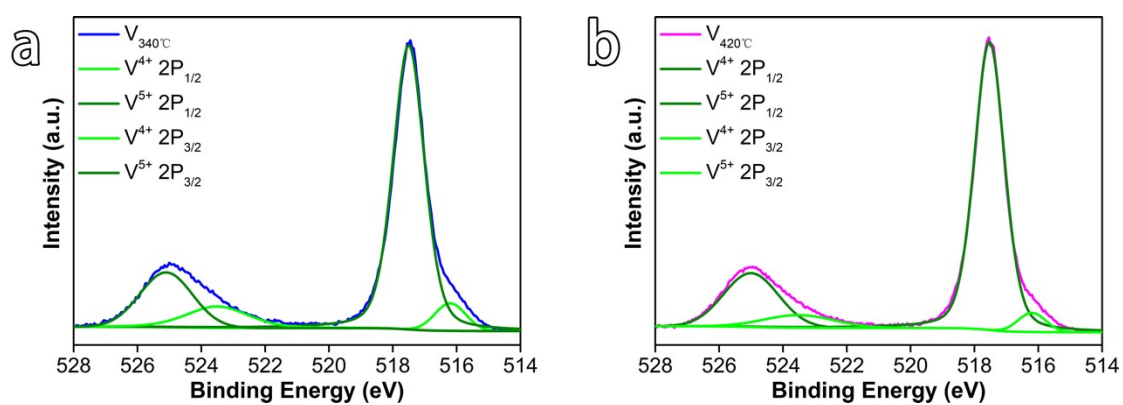


Figure S7. V_{2p} XPS of (a) V_{340°C} (blue) and (b) V_{420°C} (pink) catalysts.

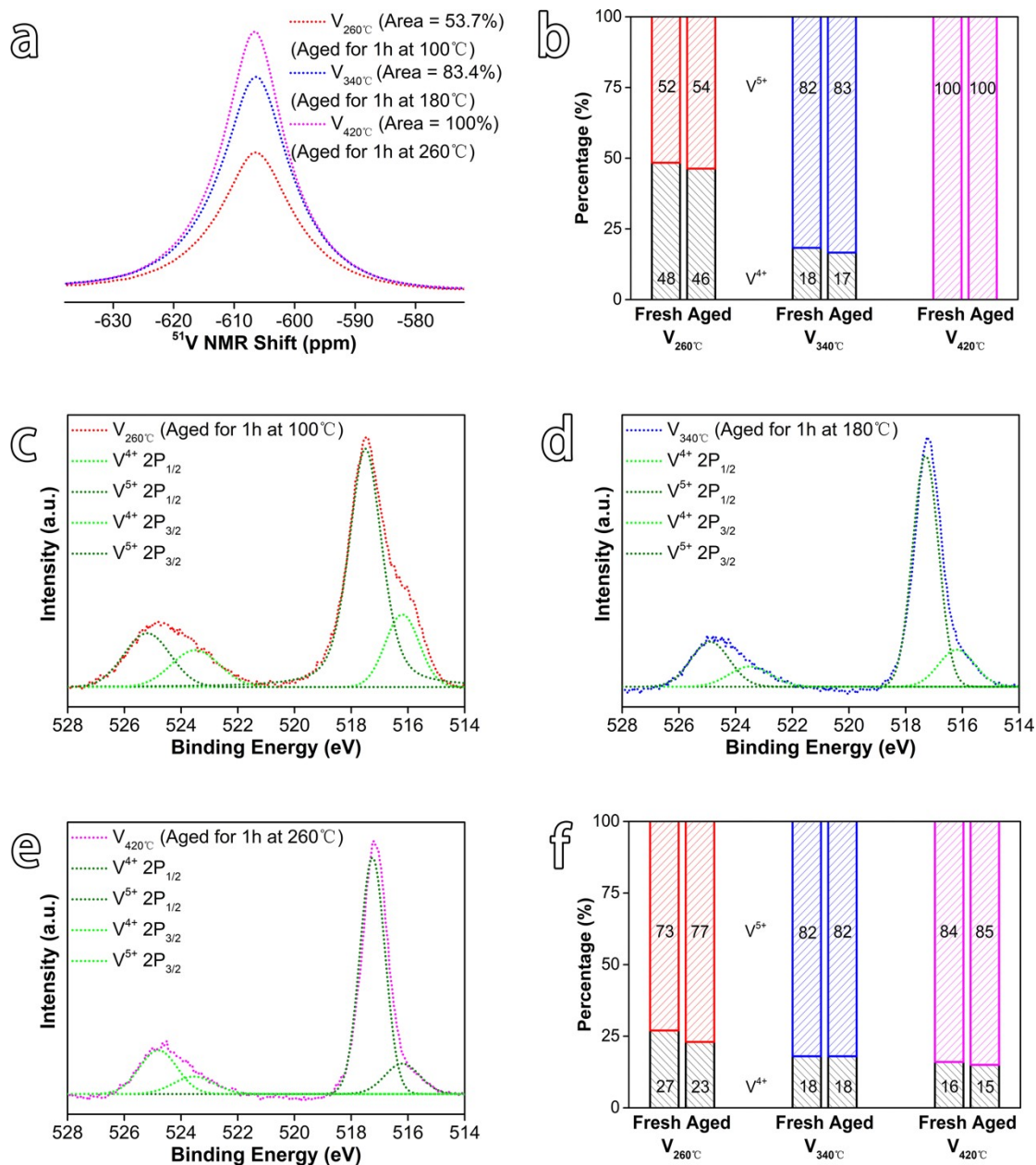


Figure S8. (a) ^{51}V NMR. (b) the V^{4+}/V^{5+} ratio in fresh and aged $V_{260^\circ\text{C}}$, $V_{340^\circ\text{C}}$, and $V_{420^\circ\text{C}}$ catalysts inferred by NMR. (c - e) V_{2P} XPS of $V_{260^\circ\text{C}}$ (red), $V_{340^\circ\text{C}}$ (blue), and $V_{420^\circ\text{C}}$ (pink) catalysts after aging. (f) V^{4+}/V^{5+} ratio in fresh and aged $V_{260^\circ\text{C}}$, $V_{340^\circ\text{C}}$, and $V_{420^\circ\text{C}}$ catalysts inferred by XPS.

There are two reasons for the difference in the activity of $V_{340^\circ\text{C}}$ and $V_{420^\circ\text{C}}$ catalysts, although the V^{4+}/V^{5+} ratio of $V_{340^\circ\text{C}}$ catalyst is similar to that of $V_{420^\circ\text{C}}$ catalyst on the surface. On the one hand, because the activity is related to the surface structure, but not only to that, the proportion of the surface V^{4+} and V^{5+} must be affected by the proportion of the body phase V^{4+} and V^{5+} , $V_{340^\circ\text{C}}$ catalyst has a certain amount of V^{4+} in the body phase, so when the surface V goes through the change of V^{3+} , V^{5+} , V^{4+} , and V^{5+} , it can change back more quickly and complete a catalytic cycle, while $V_{420^\circ\text{C}}$ catalyst is almost all V^{5+} , so it is difficult to change from V^{3+} to V^{5+} . Therefore, compared with $V_{340^\circ\text{C}}$ catalyst, $V_{420^\circ\text{C}}$ catalyst is more difficult to exchange oxygen at low temperature in Figure 6b and not easy to complete the structural cycle. On the other hand, the XPS used in this paper is a kind of *non-in-situ* test, and the surface V^{4+}/V^{5+} ratio is inevitably affected by air. The XPS test results

can only provide reference and do not have a decisive significance. XPS, NMR, DFT and EXAFS together can infer that a higher proportion of V^{4+} is beneficial to low temperature activity.

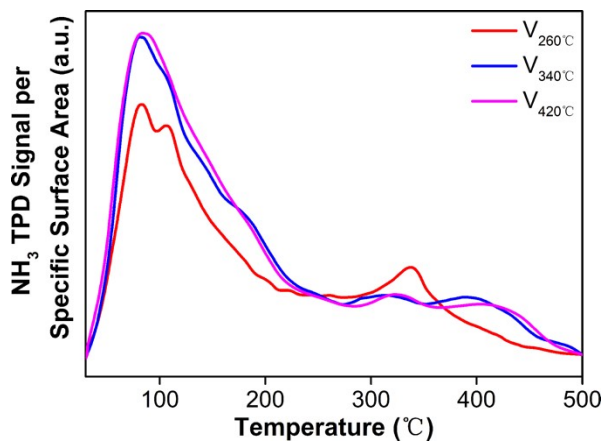


Figure S9. NH_3 -TPD per specific surface area of $V_{260^\circ C}$ (red), $V_{340^\circ C}$ (blue), and $V_{420^\circ C}$ (pink) catalysts.

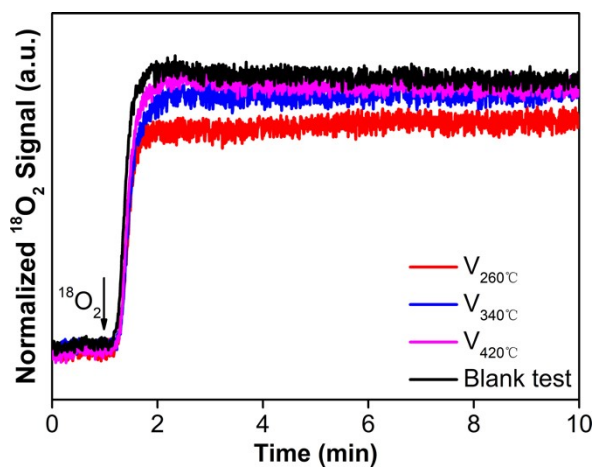


Figure S10. Signal of $^{18}O_2$ during $^{18}O_2$ isotope exchange.